

## Fission following fusion of Ni + Sn

K. T. Lesko,\* W. Henning, K. E. Rehm, G. Rosner,<sup>†</sup> J. P. Schiffer,  
G. S. F. Stephans,<sup>‡</sup> and B. Zeidman  
*Argonne National Laboratory, Argonne, Illinois 60439*

W. S. Freeman

*Fermi National Accelerator Center, Batavia, Illinois 60510*

(Received 12 May 1986)

Excitation functions for fission were measured for  $^{58,64}\text{Ni}$  beams incident on the even  $^{112-124}\text{Sn}$  targets at energies extending from well below to about 1.5 times the Coulomb barrier. Fission was identified by kinematic coincidence between fission fragments. Angle integrated fission cross sections were obtained from angular distributions taken at several energies for all systems. From these and the previously measured cross sections for evaporation residues, we obtain the total fusion cross sections and fission probabilities over the energy range  $150 \leq E_{\text{c.m.}} \leq 240$  MeV. The competition between particle evaporation and fission in the compound nuclei is compared to statistical model calculations. A good description of the data for all 14 systems is achieved with the use of a single set of parameters. The model includes fission barriers with finite range and nuclear diffuseness effects, and partial-wave distributions for fusion that are qualitatively consistent with those from microscopic reaction model calculations. The fusion excitation functions are analyzed in terms of the dynamical fusion model of Swiatecki *et al.* Within this model we extract new values for the "extra-push" parameters.

## I. INTRODUCTION

Heavy ion fusion reactions have allowed the study of the properties of nuclei with large angular momenta for many years. This is, however, most often accompanied by considerable internal excitation energy (temperature). For a given compound nucleus, the maximum angular momentum that can generally be reached at a fixed excitation energy is obtained through near-symmetric entrance channels. This is illustrated for a Pt compound nucleus in Fig. 1, where we have plotted the maximum angular momentum (corresponding to a grazing collision) versus excitation energy for various entrance channels. The dependence of the properties of the compound nucleus on angular momentum and temperature can thus be studied by appropriate choices of the entrance channel system. In particular, for cold high-spin nuclei with excitation energies in the vicinity of the yrast line, nuclear structure effects may be important in the competition between particle and fission decay.

We have chosen to study in a systematic fashion a series of Pt compound nuclei whose neutron excesses,  $N - Z$ , vary by about a factor of 2, and which are populated through fusion reactions with large angular momenta at relatively low excitation energies. This was achieved by selecting the near-symmetric entrance channels Ni + Sn, for which  $A_{\text{proj}} \geq \frac{1}{2} A_{\text{target}}$ . In these systems, compound nuclei are produced at excitation energies typically 20–50 MeV closer to the yrast line than in other recent experiments where both the evaporation residues and the fission fragments were observed.<sup>1–5</sup> With a near-symmetric entrance channel it can be difficult to resolve

the masses of the fission fragments from those of the target and projectile nuclei. This difficulty was solved by requiring a kinematic coincidence between the fission fragments and additional measurements of the parameters of the individual ions.

The fission data which we present here for the systems  $^{58,64}\text{Ni} + \text{even Sn}$  isotopes between  $^{112}\text{Sn}$  and  $^{124}\text{Sn}$  complement an earlier study of the fusion residues for the same systems over the same energy range.<sup>6</sup> Those mea-

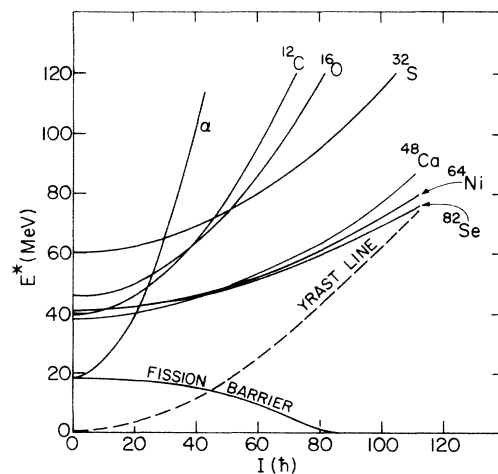


FIG. 1. The maximum angular momentum  $I$  (corresponding to a grazing collision) versus excitation energy  $E^*$  for the compound nucleus  $^{188}\text{Pt}$  formed through various entrance channels labeled by the projectile nucleus.

surements demonstrated a dramatic dependence upon neutron excess of the maximum cross sections for leaving evaporation residues, with the cross sections increasing by an order of magnitude from the most neutron-deficient to the most neutron-rich Pt nucleus. Attempts to reproduce the mass dependence of this trend through statistical model calculations resulted in a qualitative agreement. However, using standard default parameters for level densities, rotating-liquid drop masses, fission barriers, etc., the statistical model code CASCADE (Ref. 7) underpredicted the observed increase by a factor of 2. These differences between the model predictions and observed evaporation residue yields might be explained either by differences in the total compound nucleus production (fusion) cross sections, or by differences in competition between fission and evaporation for the systems which were not accounted for in the standard statistical model calculations. By measuring the fission cross sections for the same systems,  $^{170-188}\text{Pt}$ , we have now directly determined the fusion cross sections.

The sum of the cross sections for leaving evaporation residues and for fission is, by definition, the total compound nucleus or fusion cross section. Consequently, the fission cross section divided by this sum represents the probability that the compound system, once formed, decays by fission. These data provide a good opportunity to test theoretical models of the fission barrier heights since both the fission and evaporation cross sections were determined experimentally and one does not have to rely upon model predictions for the total fusion cross sections. Moreover, the data cover a large range in neutron excess corresponding to a wide range in fissility. The use of the two different beams on the different Sn targets leads in several cases to the production of the same compound nucleus with nearly the same excitation energy, but with different angular momentum distributions. A partial analysis of the present data in terms of the competition between fission and light-particle decay has been published previously.<sup>8</sup>

Finally, having experimentally measured the compound nucleus cross sections, we can investigate aspects of the fusion dynamics by comparing to the “extra-push” parametrization of Swiatecki.<sup>9</sup> Our range in fissility provides a good opportunity to test the validity of this and similar models. The particular systems investigated here populate nuclei which are near the expected threshold region for the onset of an extra push.

## II. EXPERIMENTAL PROCEDURE

### A. Fission measurements

Excitation functions for fission were measured over the energy range  $150 \leq E_{c.m.} \leq 240$  MeV for  $^{58}\text{Ni}$ , and  $150 \leq E_{c.m.} \leq 200$  MeV for  $^{64}\text{Ni}$ , with beams from the Argonne Tandem-Linac Accelerator (ATLAS). The energy resolution of the linac beam was about 2 MeV (FWHM). Together with target thickness effects this leads to an estimated overall uncertainty of  $\approx \pm 1$  MeV in the energy centroids for the excitation functions. The kinematics of the Ni + Sn reactions are such that a singles measurement

with finite mass and charge resolution could not separate fission products from deep-inelastic events. To unambiguously determine the fission cross sections we employed a coincident-fragment detection scheme. One fission fragment was detected in a gas- $\Delta E$ , silicon surface barrier- $E$  detector telescope with time-of-flight measured between the linac beam pulse and the silicon- $E$  detector signal. With a flight path of 27.8 cm we obtained a mass resolution of 8 u for mass  $\sim 90$  fragments. The charge of the fragment was deduced from the differential energy loss measurement in the gas  $\Delta E$  detector, with a resolution of  $\Delta Z \approx 2$ . The acceptance of the  $\Delta E$ - $E$  TOF spectrometer was determined by the defining aperture and measured to be 0.64 msr.

The coincident fragment was detected in a large area position-sensitive gas detector originally constructed at the Max-Planck-Institut in Heidelberg.<sup>10</sup> In addition to recording the angles in both the azimuthal and the reaction planes, the detector measured the differential energy loss of particles and thereby allowed one to deduce the charge of the detected fission fragments to within  $\Delta Z \approx 2-5$  depending on fission fragment energy. The kinematics for the range of mass divisions in the fission events resulted in a spread of coincident fragments through an angular cone with a half-angle of approximately 8 deg in the laboratory. The detector spanned 35 deg in the reaction plane and 17 deg perpendicular to it, thereby assuring acceptance of all coincident fragments, except for a known 15% correction from the wire grid supporting the entrance foil.

We measured the mass, charge, position, and energy of one fission fragment and the position, charge, and energy of the coincident fragment. This represents an overdetermination of binary decay processes, but was necessary to distinguish fission events at low incident energies, where fission cross sections are small, from large backgrounds of inelastic events. Fission following “incomplete fusion” (where a component of the projectile is not captured by the target) would be included in the fission yield. Such processes, however, are thought to be unimportant for this mass and energy range.<sup>11</sup>

### B. Fission cross sections

Angular distributions of fission fragments were measured for all systems at several energies. These distributions approached the expected  $1/\sin(\theta)$  dependence of the fission distributions at the higher energies. We calculated corrections to the assumed distributions using predictions obtained from the statistical model of fission which relied on fission saddle-point shapes predicted by the rotating liquid drop model<sup>12</sup> (RLDM) and on estimates of the maximum angular momentum for fusion obtained from the measured fusion cross section and a sharp cutoff of the partial-wave distribution. At the higher energies these corrections are of the order of a few percent; at the lower energies the angle-integrated differences between the predicted angular distribution and a  $1/\sin(\theta)$  dependence amount to at most 25%. The effect of these corrections on the total fusion cross sections are minimal in that for the lower energies the predominant decay mode is particle

evaporation and at the higher energies, where fission dominates, the calculated corrections are within the experimental errors of the fission data.

To extract the binary fission yields the following cuts were made on the data: we required that a coincident fragment be detected in each detector; elastic and quasi-elastic events were then separated using both the charge information and the energy spectra; the fission fragment observed in the large position-sensitive detector was required to be in the kinematically correct position region for fission events (with both detectors situated near  $\theta_{c.m.} = 90$  deg, the separation in angle between symmetric fission and elastic scattering is  $\sim 3$  deg in the laboratory); and additional separation and identification of fission events from deep-inelastic transfer products was obtained from the mass spectra (calculated from the energy spectra and time-of-flight) and the sum energy of both detectors.

The data reduction relied on the overdetermination of the binary decay parameters to guarantee the fragment identification. Consequently, the individual gates provided a generous acceptance. This allowed us to use the same gates and cuts on the data for all targets at a common bombarding energy. The systematic errors were found to be  $< 8\%$  at the higher energies, but amounted to as much as  $30\%$  at the lowest energies where the fission yields were relatively low with respect to the number of background events. The measured fission excitation functions are plotted in Fig. 2. The errors shown are from the systematic uncertainties in the gating procedure. At higher energies, where these uncertainties are less than  $8\%$ , the overall errors in the fission cross sections were estimated to be  $\pm 10\%$ .

### C. Fusion cross sections and fission probabilities

In order to deduce the total fusion cross sections from the separate measurements of fission and evaporation residues, we needed to interpolate between the two data sets to common center-of-mass energies. In Figs. 3 and 4 we have plotted both the present fission cross sections and the previously measured cross sections<sup>6</sup> for fusion residues after light particle evaporation. The curves through the data points are the results of model calculations discussed in Sec. III A.

At the lower energies where the cross sections for leaving evaporation residues dominate, the fission data were linearly interpolated and added to the experimental values for the residues; at the higher energies where fission is largest, the evaporation residue data were interpolated and added to the fission data points. In Figs. 5 and 6 the resulting fusion excitation functions are plotted. Again, the curves through the data points are the results of calculations discussed in Sec. III.

From the measurements of fission and the total fusion cross sections, we can obtain the fission probability by taking the ratio of these two quantities. The fission probability will be used to examine various fission barrier height parametrizations. These probabilities span several decades in cross section and extend from a region of low spin and excitation where particle evaporation dominates, to a region of high spin and higher excitation where fis-

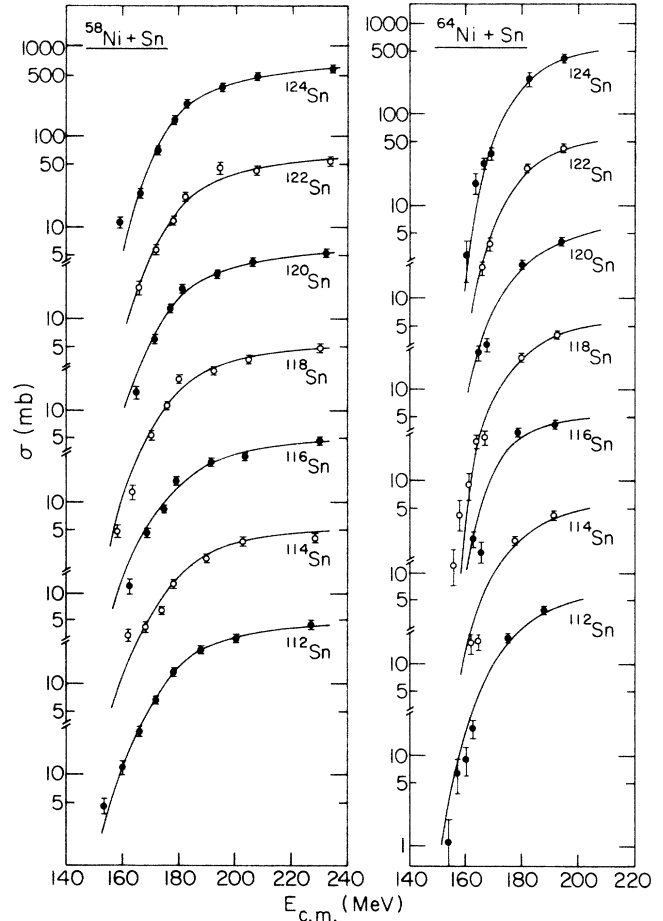


FIG. 2. Experimental fission cross sections for  $^{58,64}\text{Ni} + ^{112-124}\text{Sn}$ . The curves are the results of statistical model calculations discussed in the text.

sion is essentially the only decay mode. At the lower excitation energies, the fission probability is rather sensitive to the spin distribution of the compound nucleus. The fission data, therefore, also allow a determination of the fusion spin distribution. The latter has been extensively alluded to in the recent work in sub-Coulomb fusion reactions,<sup>13</sup> as will be discussed below in more detail.

## III. COMPARISON WITH MODELS

### A. Statistical model calculations of compound nucleus decay

The initial attempts to reproduce, for the present systems, the cross sections for leaving a fusion residue after particle evaporation were unsuccessful.<sup>6</sup> In these first calculations we used calculated fusion cross sections and the standard version of the statistical model code CASCADE.<sup>7</sup> While the observed trends of increasing maximum cross sections for particle evaporation as a function of neutron number were reproduced, the increase was too small by about a factor of 2. "Standard" input parameters were used in those calculations: notably a value of the fission barrier height of 85% of the usual RLDM prediction, a

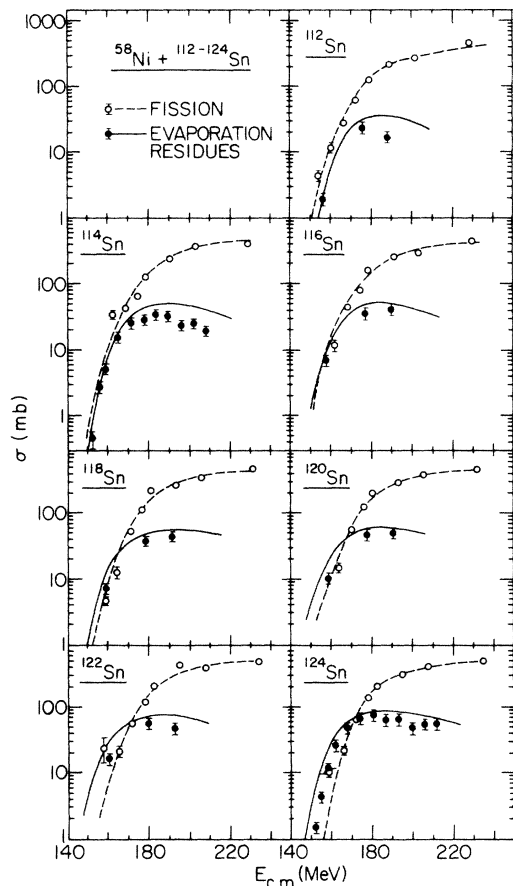


FIG. 3. Experimental fission (open circles) and evaporation residues cross sections (closed circles) for the systems  $^{58}\text{Ni} + ^{112-124}\text{Sn}$ . The curves are statistical model predictions discussed in the text.

sharp cutoff in the angular momentum distribution, and compound nuclear cross sections calculated from the Bass model.<sup>14</sup>

Since the first analysis, significant progress has been made in the calculation of fission barrier heights using a rotating liquid drop model. Sierk has introduced a new semiempirical expression which incorporates effects from the finite range of the nuclear force and the diffuseness of the nuclear surface.<sup>15</sup> These modifications have been successful in modeling recent fission data without the need to resort to an arbitrary reduction factor for the barrier height in rotating liquid drop model calculations.<sup>16</sup> We have incorporated the new fission barriers of Sierk into the CASCADE code.

In addition to these new barriers, several other parameters need to be chosen. Of particular importance in modeling the competition between fission and particle evaporation is the choice of the level density parameters,  $a_f$  and  $a_n$ , which determine the level densities at the ground state and saddle point. Bishop<sup>17</sup> *et al.* have proposed a simple model for predicting the dependence of the single-particle level densities on deformation. When the effects from the diffuse surface are included, ratios of

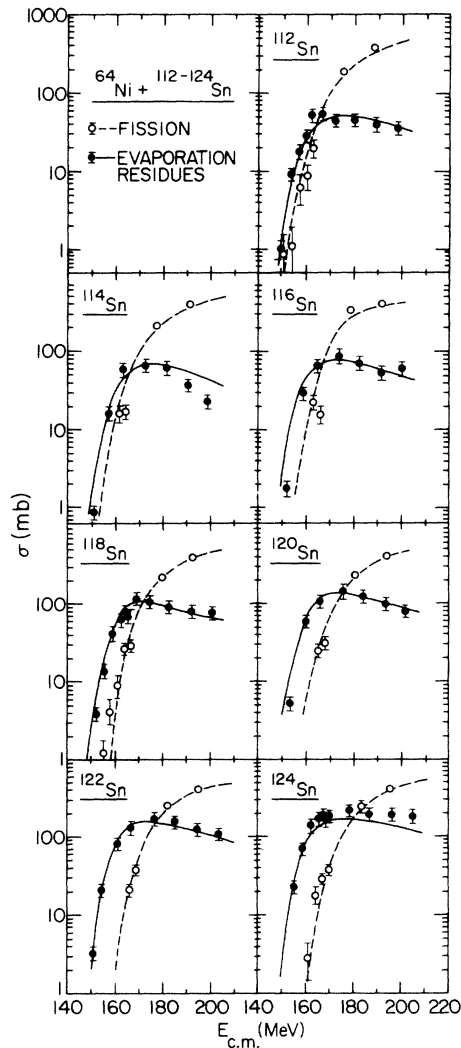


FIG. 4. Experimental fission (open circles) and evaporation residues cross sections (closed circles) for the systems  $^{64}\text{Ni} + ^{112-124}\text{Sn}$ . The curves are statistical model predictions discussed in the text.

$a_f/a_n$  slightly larger than one are obtained. Using these equations we have calculated the values of  $a_f/a_n$  for the two extremes in neutron excess,  $^{170}\text{Pt}$  and  $^{188}\text{Pt}$ , and find them to lie between 1.02 and 1.04. We then investigated the effect introduced into the statistical model predictions by this range of level density ratios and found the effects on the fission probability to be within experimental uncertainties. For this reason and in order to keep the computational effort at a reasonable level, we have assumed  $(a_f/a_n)=1.0$ . For  $a_n$  we have chosen the generally accepted value  $a_n = A/8.0$  ( $\text{MeV}^{-1}$ ).

For the RLDM masses used in the statistical model we have chosen the Myers droplet parametrization with the Wigner term.<sup>18</sup> This term has its origin in the shell model, but is not a shell correction in the usual sense. The term arises from the increased overlap of wave functions of particles in identical orbits, including all closed shells, and thus represents a bulk property of the nucleus.

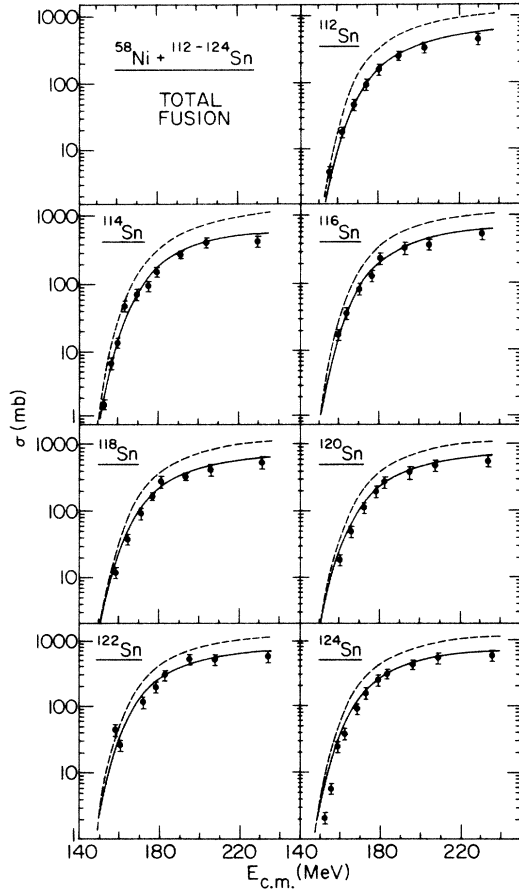


FIG. 5. Experimental fusion cross sections for  $^{58}\text{Ni} + ^{112-124}\text{Sn}$ . The solid points are the measured total compound nucleus formation cross sections for the systems  $^{58}\text{Ni} + ^{112-124}\text{Sn}$ . The solid and dashed curves are model predictions with and without extra push.

The Wigner term is proportional to  $(N - Z)$ , and thus becomes more important in heavy nuclei. Our initial calculations using the default option in CASCADE (which does not include the Wigner term) overestimated the fission cross sections considerably.

Another quantity that strongly affects the statistical model predictions is the partial-wave distribution of the compound nucleus. Indeed, the large body of data obtained in this work allows a systematic study of this distribution. The sharp cutoff model has been generally used as a first estimate of the angular momentum populations through

$$\sigma_{\text{fus}} = \pi\lambda^2 \sum_l (2l + 1) T_l(E), \quad (1)$$

where  $T_l$  is the transmission coefficient for the partial-wave  $l$ . In the sharp cutoff approximation

$$\begin{aligned} T_l(E) &= 1; \quad l \leq l_{\text{cr}} \\ &= 0; \quad l > l_{\text{cr}}, \end{aligned} \quad (2)$$

yielding a simple expression for the fusion cross section in terms of a critical angular momentum,  $l_{\text{cr}}$ . In recent

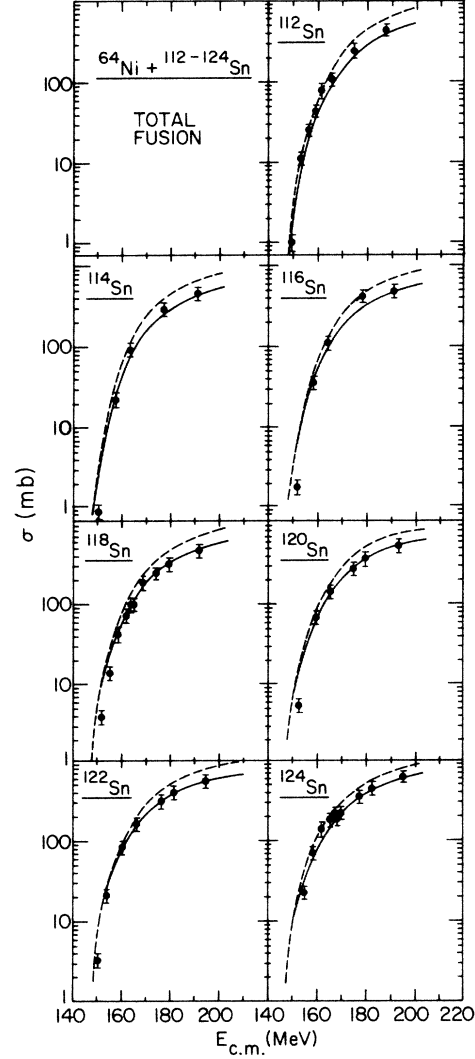


FIG. 6. Experimental fusion cross sections for  $^{64}\text{Ni} + ^{112-124}\text{Sn}$ . The solid points are the measured total compound nucleus formation cross sections for the systems  $^{64}\text{Ni} + ^{112-124}\text{Sn}$ . The solid and dashed curves are model predictions with and without extra push.

work by Vandenbosch *et al.*<sup>19</sup> angular momentum distributions have been measured with a variety of techniques; their results strongly indicate the inadequacy of such an approximation. In addition, the recent work on the energy dependence of fusion cross sections below the barrier also stresses a diffuse partial-wave distribution.<sup>13</sup> We have therefore chosen to represent the partial-wave distribution of the entrance channel transmission coefficients by a Fermi function dependence

$$T_l = 1 / \{ 1 + \exp[2(l - l_0)/\sigma] \}, \quad (3)$$

where  $\sigma$  is the additional parameter representing the diffuseness (approximately the interval in which the distribution falls from  $\sim 80\%$  to  $\sim 20\%$  of its peak value at the high spin end). We searched for the value of  $\sigma$  to best fit all present data on the fission probabilities. The other

quantity constraining the angular momentum distribution is the fusion cross section which we measured directly (Figs. 5 and 6). In order to smooth out the experimental fluctuations in the total fusion data for this purpose, we used the solid curves in Figs. 5 and 6 which are the results of the fusion model calculations discussed in Sec. III D.

For a reasonable description of all our data we found a clear need to use the fission barrier treatment of Ref. 15 and to optimize the parameter  $\sigma$  of the partial-wave distribution. The dependence of the fission probability on these parameters was illustrated for one of the systems,  $^{64}\text{Ni} + ^{124}\text{Sn}$ , in our partial analysis which was published previously.<sup>8</sup> The sensitivity to  $\sigma$ , a single fixed parameter for all systems, is further illustrated by an experimental quantity which can be readily extracted from the data, namely the crossover energy, i.e., the excitation energy in the compound nucleus at which the cross section for fission is equal to the cross section for leaving an evaporation residue. In Fig. 7 the experimental crossover energies for all 14 systems are plotted. For the lightest system,  $^{58}\text{Ni} + ^{112}\text{Sn}$ , we did not measure the cross sections at low enough energies to observe the crossover energy, if it indeed exists, and the data point shown is an extrapolation. Also shown in the figure are the crossover energies calculated with several choices of  $\sigma$ . The sensitivity to  $\sigma$  is apparent, especially for the lighter systems. We have required  $\sigma$  to be fixed, although there is no *a priori* reason for this, but large variations might be surprising in view of the structural similarity of the collision systems (see the discussions below).

The value of  $\chi^2$  obtained with the measured fission probabilities compared to the calculations for all 14 systems is at a minimum when a value of  $\sigma = 15\hbar$  is used, as is illustrated in Fig. 8. Furthermore, in Fig. 7 it can be seen that this value gives an acceptable fit to crossover energies for the compound systems induced by both  $^{58}\text{Ni}$  and  $^{64}\text{Ni}$ .

In Figs. 3 and 4 the predicted evaporation and fission cross sections are summarized together with the data for

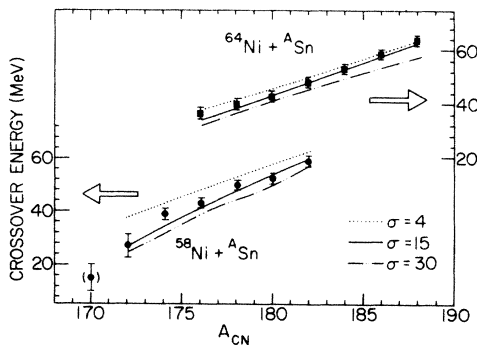


FIG. 7. Compound nucleus mass dependence of the crossover energy where fission and particle evaporation cross sections are equal. The squares (circles) indicate the experimentally determined crossovers for the systems formed with  $^{64}\text{Ni}$  ( $^{58}\text{Ni}$ ) beams. The different curves indicate model predictions with different values of the diffuseness parameter  $\sigma$  for the fusion partial-wave distribution.

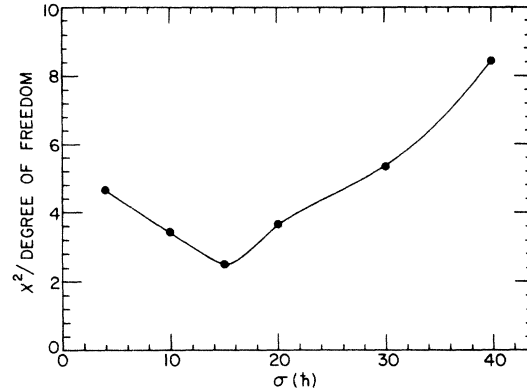


FIG. 8. The  $\chi^2$  value of statistical model predictions compared to experimentally determined fission probabilities for the systems  $^{58,64}\text{Ni} + ^{112-124}\text{Sn}$  as a function of the diffuseness parameter  $\sigma$ .

all the systems which we have studied. Again, the solid circles are the experimental evaporation cross sections, the open circles refer to the fission cross sections, and the curves are the model predictions for these two quantities with the optimum parameters discussed above. Similarly, the curves through the fission excitation functions in Fig. 2 are the results of the same calculations.

### B. Sub-barrier fusion cross sections

As indicated above, a separate quantity which is sensitive to the shape of the fusion partial-wave distribution is the fusion cross section at sub-barrier energies. The enhancement has generally been interpreted as due to a change of the interaction potential through coupling of the elastic channel to other quasi-elastic degrees of freedom.

At the lower energies the present data also indicate an enhancement in cross section over a simple one-dimensional barrier penetration calculation prediction. This is illustrated in Fig. 9 for the system  $^{58}\text{Ni} + ^{124}\text{Sn}$ . The curves are the results of reaction calculations from the microscopic coupled-channels code PTOLEMY,<sup>20</sup> with and without coupling of inelastic excitations of both projectile and target to the elastic channel. In these calculations, the real part of an optical model potential that fits elastic scattering data of 330 MeV  $^{58}\text{Ni}$  on  $^{116}\text{Sn}$  in a coupled-channels calculation with PTOLEMY was used as the basis of our calculations,<sup>21</sup> the imaginary part being set to zero. The incoming wave boundary condition (IWBC) was used as a measure of the partial waves that penetrate to sufficiently small radii to fuse. The dashed curve in Fig. 9 is the result of the calculation without couplings, the solid curve is the prediction when the coupling of the first  $2^+$  and  $3^-$  states in both Ni and Sn is included, using observed  $B(E\lambda)$ 's and form factors taken as the derivative of the real potential. While it is apparent from the two calculations in Fig. 9 that coupling to inelastic channels increases the sub-barrier fusion yields by as much as an order of magnitude, this is still not sufficient to describe the experimentally observed yields. From our

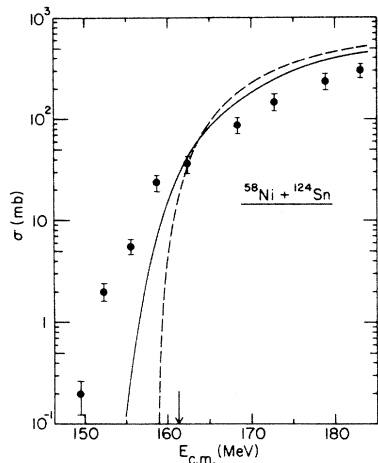


FIG. 9. Sub-barrier fusion cross section for the system  $^{58}\text{Ni} + ^{124}\text{Sn}$ . The solid (dashed) curves are model predictions from the coupled-channels reaction code PTOLEMY with (without) coupling between elastic and inelastic scattering channels. The arrow indicates the Coulomb barrier energy.

measurements of quasi-elastic transfer strengths in the same Ni + Sn systems<sup>21</sup> and our studies of sub-barrier transfer strengths in other systems,<sup>22</sup> we believe that the additional fusion enhancement is most likely due to coupling to nucleon transfer channels.

PTOLEMY does not handle the coupling of transfer channels. In addition, the detailed microscopic calculation carried out for just one system,  $^{58}\text{Ni} + ^{124}\text{Sn}$ , is quite time consuming. We have therefore used the more schematic and analytical model of Esbensen *et al.*<sup>23</sup> to calculate fusion cross sections in the barrier region for all systems.

In this model, collective surface vibrations are considered as the important inelastic channels, and their effect on sub-barrier fusion is treated by introducing variations in the surface separation and in the effective fusion barrier height. The relevant parameter in this model is  $\sigma_\lambda$ , the standard deviation of surface fluctuations due to a collective vibration of multipolarity  $\lambda$ . When several surface modes are important, their contributions and resulting reductions of the Coulomb barrier are added. Using the formulas from Ref. 23 for the Ni + Sn systems, we calculate average total values  $\sigma_\lambda$  between 0.2 to 0.3 from known reduced transition strengths  $B(E\lambda)$  to low-lying collective states ( $2^+$ ,  $3^-$ ,  $4^+$ ,  $5^-$ ) in both Sn and Ni nuclei. In order to reproduce in the average the total fusion excitation function below and near the barrier for our systems, however, a value 2–3 times larger is needed. We believe that this again reflects the importance of transfer channels in the sub-barrier enhancement. We have empirically selected a value of  $\sigma_\lambda = 0.7$  for all 14 fusion excitation functions. The underlying fusion cross sections without barrier variations were taken from the classical model by Swiatecki.<sup>9</sup> This is discussed in more detail in Sec. III D, where the final results are presented.

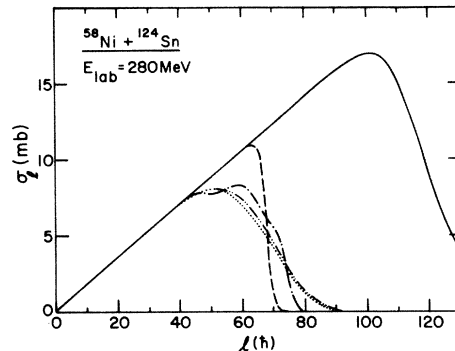


FIG. 10. Calculated partial-wave cross section distributions for the system  $^{58}\text{Ni} + ^{124}\text{Sn}$ . The solid curve is an optical-model prediction of the total reaction cross section; the dashed curve is the fusion cross section calculated with the same real part of the optical-model potential and the incoming wave boundary condition; the dot-dashed curve shows the additional effect of coupling to inelastic states ( $2^+$  and  $3^-$  in both nuclei), while the double-dot-dashed curve is a result of the schematic model of Esbensen; the dotted curve represents the partial-wave distribution deduced from the fission data by way of the statistical model calculations.

### C. Partial-wave distributions

We can now compare the partial-wave distributions obtained from the model calculations of the sub-barrier fusion cross sections with the ones obtained from the statistical model fits to the ratios of fission to particle-evaporation widths. Figure 10 summarizes these results. The solid line shows the partial-wave distribution of the total reaction cross section calculated from the optical model potential that fits elastic scattering data at 330 MeV of  $^{58}\text{Ni}$  on  $^{116}\text{Sn}$ . The fusion partial-wave distributions from the IWBC coupled channels calculations of the sub-barrier fusion with the microscopic coupled-channels code PTOLEMY are shown as dashed and dashed-dotted lines, respectively, for the situations of no coupling and coupling. The double-dot-dashed line represents the results from the more schematic model of Esbensen. In both coupled cases the partial-wave distribution falls off more slowly than for the case of no coupling, in qualitative agreement with the average width of the partial-wave distribution required by the fission data (dotted curve).

### D. Fusion excitation functions

Fusion of two heavy nuclei has been the subject of intense studies over the past years. A major feature that has become apparent is the inhibition of compound nucleus formation in very heavy systems due to the reaction dynamics, which are dominated in these systems by the strong repulsive Coulomb and centrifugal forces. A convenient model to calculate these effects, since it is analytically formulated in terms of general scaling parameters, is the “extra-push” model by Swiatecki<sup>9</sup> which provides expressions for the reduction in cross section at a given energy or, conversely, the increase in energy (extra push) required to reach a given value of the fusion cross section.

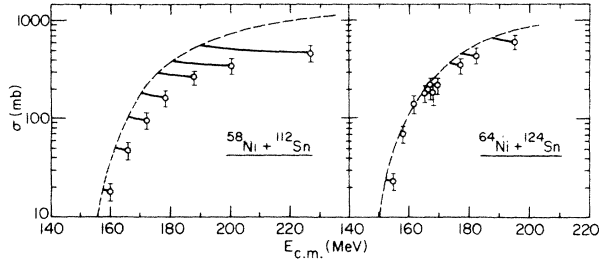


FIG. 11. Illustration of the procedure to extract “extra-push” energies. The experimental fusion cross sections (circles) are compared to fusion cross section calculations without extra push. The difference between the data and the calculated cross section curves (along lines with  $1/E_{c.m.}$  behavior) is extracted as the extra-push energy.

The Ni + Sn systems falls into the region of mass and charge where this dynamical inhibition of the fusion cross section is predicted to begin. In this sense the present data may present a sensitive test case and allow the extraction of the model parameters. The extra-push energy  $E_x$  in this model is given by<sup>9</sup>

$$E_x = E_{ch} a^2 (x - x_{th})^2, \quad (4)$$

where  $E_{ch}$  is a characteristic energy for the system and a function of the masses of the interacting nuclei;  $x$  is a normalized effective fissility, a function of the charge and mass of the interacting nuclei and of angular momentum;  $x_{th}$  is the threshold fissility above which an extra push is needed and is approximately constant; and  $a$  is a parameter giving the slope of the square root of the extra-push energy as a function of fissility.

In Fig. 11 we illustrate how the values for the extra-push energies were extracted from our data. In Fig. 12 we plot the square root of these values of the extra-push ener-

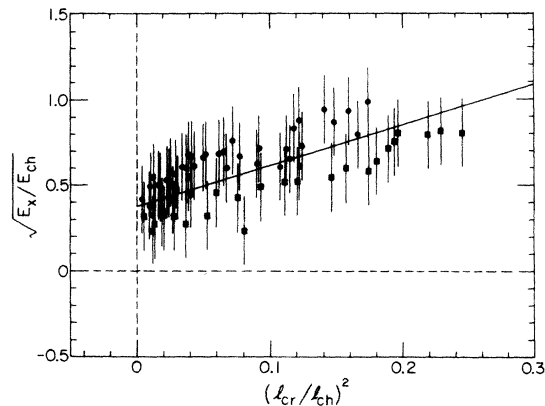


FIG. 12. Determination of the zero angular-momentum extra-push energy. The square root of the experimental extra-push energies are plotted as a function of the angular momentum squared for all systems (in units of “characteristic” channel energy  $E_{ch}$  and angular momentum  $l_{ch}$  as defined in Ref. 9). The solid circles (squares) refer to  $^{58}\text{Ni}$  ( $^{64}\text{Ni}$ ) induced reactions. In the actual analysis a straight line was fit to each collision system separately (see the text).

gies as a function of the square of the critical angular momentum  $l_{cr}$  deduced from the fusion cross sections in the sharp cutoff approximation. All systems are plotted in the same figure to illustrate their uniform behavior, except for a systematic shift which is observed between the  $^{58}\text{Ni}$  (dots) and  $^{64}\text{Ni}$  (squares) induced reactions. In the actual analysis we fitted a straight line to the data points of each separate system and extracted the intercept, which is the extrapolated value of the effective fissility at zero angular momentum,  $x_e$ , and the slope which, within the model, is equal to  $af^2$ . Here  $f$  is the “effective angular momentum fraction,” i.e., that fraction of angular momentum responsible for the centrifugal force in the separation degree of freedom.<sup>9</sup> The extra-push energy as a function of  $x_e$  is shown in Fig. 13. Within the model, a fit of a straight line to these data points yields the threshold fissility  $x_{th}$  and the slope parameter  $a$ . We obtain the following values:  $x_{th} = 0.62$ ,  $a = 5.7$ ,  $f = 0.64$  with large errors of about 30%.

The values differ from previous ones; for example, the values recently extracted by Toke *et al.*<sup>24</sup> from measurements with  $^{208}\text{Pb}$  and  $^{238}\text{U}$  beams. This might be due to the large error bars in our values or might indicate a problem with the scaling of the extra-push parameters over a large mass range. Bjørnholm and Swiatecki<sup>9</sup> have argued that a fissility  $x_m$  which is intermediate between the effective fissility  $x_e$  defined above and the fissility defined by the RLDM, might be more appropriate for a general scaling behavior of the parameters describing compound nucleus formation (the extra-extra-push formalism). Recently Back<sup>25</sup> published an analysis of data in this parametrization. If we include our data and repeat the analysis (Fig. 14), we obtain values for  $x_{th}$  and  $a$  which are not significantly different from the ones above and are rather similar to those from Ref. 25. In the two parametrizations, extra-push and extra-extra-push, the values of  $x_{th}$  and  $a$  should be the same. This is essentially the case with the latter values being  $x_{th} = 0.64 \pm 0.05$ ,  $a = 7.8 \pm 0.6$ ,  $f = 0.55 \pm 0.05$ .

The value of  $x_{th}$  is smaller than previously expected,<sup>9</sup> suggesting an earlier onset of the dynamical inhibition of

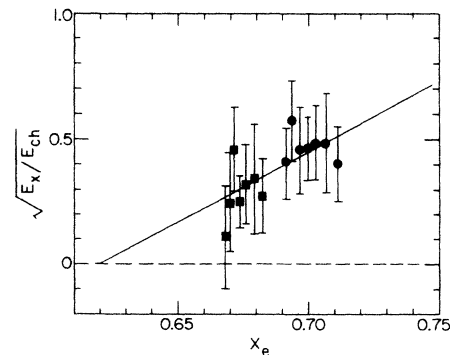


FIG. 13. The zero angular-momentum extra-push energies are plotted as a function of the effective fissility  $x_e$ . A straight line fit to the data yields the parameters of the extra-push model (see the text).

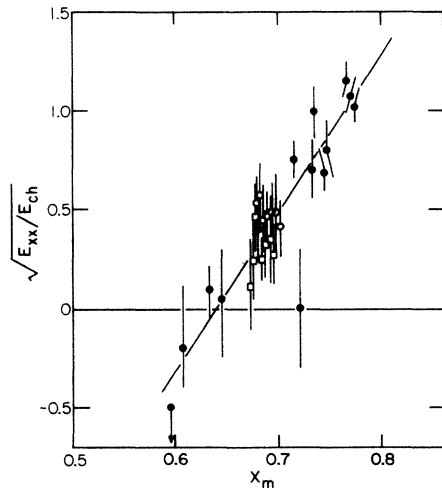


FIG. 14. A reevaluation of the extra-push energies using the extra-extra-push model. The extra-push energies are plotted versus the mean effective fissility  $x_m$ . We have plotted our data (open circles and squares) along with those of Ref. 25. From the straight line fit to these data we extract the model parameters as discussed in the text.

fusion in heavy systems. In terms of heavy-element production this emphasizes the need to go to asymmetric entrance channels in attempts to produce very heavy nuclei. The value of the slope parameter,  $a$ , which is also lower than that previously discussed, suggests a reduced dissipation constant, lower than the ones generally assumed in collision theories with one-body dissipation.<sup>26</sup>

With these parameters, theoretical fusion cross sections can now be predicted within the extra-push model.<sup>9</sup> The curves in Figs. 5 and 6 are such predictions, modified to include the barrier fluctuations discussed in Sec. III B. To do this the average potential barrier, calculated from the Yukawa potential parameters of Moeller and Nix,<sup>27</sup> was varied according to the schematical coupling model of Esbensen discussed in Sec. III B. The fusion cross section for this range of barriers was then correspondingly averaged. At low energies, the fusion cross section is essentially determined by the barrier fluctuations, as expected from our discussion in Sec. III B. At the higher energies the cross section curves are essentially those of the classical model, without (dashed curve) and with (solid curve) extra push.

#### IV. CONCLUSIONS

We have measured the fission excitation functions for the systems  $^{58,64}\text{Ni} + ^{112-124}\text{Sn}$ . Combining these measurements with the previously measured evaporation residue cross sections, we have obtained the total fusion cross sections for a series of isotopes whose neutron excess,  $N - Z$ , varies by nearly a factor of 2. This has provided us with a sensitive tool to examine the neutron-excess and angular-momentum dependence of the competition between fission and particle evaporation at a constant atomic number.

Using a modified version of the statistical code CASCADE, we have shown that the new fission barriers of Sierk provide a good description of the competition between fission decay and particle evaporation within the framework of the statistical model. We have used a single set of parameters to describe all 14 excitation functions formed by the fusion of  $^{58,64}\text{Ni}$  on  $^{112-124}\text{Sn}$ . The analysis clearly reveals a diffuse cutoff in angular momentum of the compound nucleus cross section, in qualitative agreement with results from fitting the enhanced fusion cross sections at sub-barrier energies and from microscopic reaction model predictions. This analysis has further indicated that the large systematic change within the evaporation cross sections is due to difference in fission competition rather than differences in compound nucleus formation cross sections.

From the excitation functions for fusion at energies well above the barrier we have extracted parameters within the extra-push model. With this set of parameters the total fusion cross sections for all systems investigated are described reasonably well. From our set of extra-push parameters we see indications of problems either with scaling this model to different systems, or in previous attempts to extract the parameters. An analysis of the "extra-extra-push" parameters resolves these scaling problems and produces parameters which are consistent with those from an independent analysis.

The data presented in this paper have been submitted to the AIP Physics Auxiliary Publication Service.<sup>28</sup>

#### ACKNOWLEDGMENTS

We would like to thank B. Back for helpful discussions and for providing us with his extra-push computer code. This work was supported by the U.S. Department of Energy, Office of Basic Energy Sciences, under Contract W-31-109-ENG-38.

\*Present address: Lawrence Berkeley Laboratory, 1 Cyclotron Road, Berkeley, CA 94720.

†Present address: Technische Universität München, James-Frank Strasse, D-8046 Garching, Federal Republic of Germany.

‡Present address: Massachusetts Institute of Technology, 26-415, Cambridge, MA 02139.

<sup>1</sup>R. G. Stokstad *et al.*, *Z. Phys. A* **295**, 269 (1980).

<sup>2</sup>B. Sikora *et al.*, *Phys. Rev. C* **25**, 1446 (1982).

<sup>3</sup>D. J. Hinde *et al.*, *Nucl. Phys.* **A385**, 109 (1982).

<sup>4</sup>S. E. Vigdor *et al.*, *Phys. Rev. C* **26**, 1035 (1982).

<sup>5</sup>H.-G. Clerc *et al.*, *Nucl. Phys.* **A419**, 571 (1984).

<sup>6</sup>W. S. Freeman *et al.*, *Phys. Rev. Lett.* **50**, 1563 (1983).

<sup>7</sup>F. Pühlhofer, *Nucl. Phys.* **A280**, 267 (1977); and private communication.

<sup>8</sup>K. T. Lesko *et al.*, *Phys. Rev. Lett.* **55**, 803 (1985).

<sup>9</sup>W. J. Swiatecki, *Phys. Scr.* **24**, 113 (1981); *Nucl. Phys.* **A376**, 275 (1982); S. Bjørnholm and W. J. Swiatecki, *ibid.* **A391**, 471

- (1982).
- <sup>10</sup>G. Rosner *et al.*, Nucl. Instrum. Methods **188**, 561 (1981); B. Heck *et al.*, Max-Planck-Institut, Heidelberg, Annual Report 1980 (unpublished), p. 25.
- <sup>11</sup>G. F. S. Stephans *et al.*, Phys. Lett. **161B**, 60 (1985).
- <sup>12</sup>S. Cohen, F. Plasil, and W. J. Swiatecki, Ann. Phys. (N.Y.) **82**, 557 (1974).
- <sup>13</sup>For a recent review, see, for example: *Fusion Reactions Below the Coulomb Barrier*, Vol. 219 of *Lecture Notes in Physics*, edited by S. G. Steadman (Springer, New York, 1984).
- <sup>14</sup>R. Bass, Nucl. Phys. **A231**, 45 (1974).
- <sup>15</sup>A. J. Krappe, J. R. Nix, and A. Sierk, Phys. Rev. C **20**, 992 (1979); A. Sierk, private communication.
- <sup>16</sup>J. van der Plicht *et al.*, Phys. Rev. C **28**, 2022 (1983).
- <sup>17</sup>C. J. Bishop, I. Halpern, R. W. Shaw, Jr., and R. Vandenbosch, Nucl. Phys. **A198**, 161 (1972).
- <sup>18</sup>W. D. Myers, *Droplet Model of the Atomic Nucleus* (IFI/Plenum, New York, 1977).
- <sup>19</sup>R. Vandenbosch *et al.*, Phys. Rev. C **28**, 1161 (1983).
- <sup>20</sup>S. Pieper, M. H. Macfarlane, and M. Rhoades-Brown, Argonne Report ANL-76-11, 1976, revised.
- <sup>21</sup>A. van den Berg *et al.*, Phys. Rev. Lett. **56**, 572 (1986).
- <sup>22</sup>K. E. Rehm, F. L. H. Wolfs, A. M. van den Berg, and W. Henning, Phys. Rev. Lett. **55**, 280 (1985).
- <sup>23</sup>H. Esbensen, Nucl. Phys. **A352**, 147 (1981); H. Esbensen, Jian-Qun Wu, and G. F. Bertsch, *ibid* **A411**, 275 (1981).
- <sup>24</sup>J. Toke *et al.*, Nucl. Phys. **A440**, 327 (1985).
- <sup>25</sup>B. B. Back, Phys. Rev. C **31**, 2104 (1985).
- <sup>26</sup>R. Nix, private communication.
- <sup>27</sup>P. Moeller and J. R. Nix, Nucl. Data Tables **26**, 165 (1981).
- <sup>28</sup>See AIP document no. PAPS-PRVCA-34-2155-15 for 15 pages of Tables of Cross Sections for Compound Nucleus Formation (Fusion), Evaporation Residues, and Fission for the Systems  $^{58,64}\text{Ni} + ^{112,114,116,118,120,122,124}\text{Sn}$ . Order by PAPS number and journal reference from American Institute of Physics, Physics Auxiliary Publication Service, 335 East 45th Street, New York, N.Y. 10017. The prepaid price is \$1.50 for each microfiche (98 pages), or \$5.00 for photocopies of up to 30 pages, and 15¢ for each additional page over 30 pages. Air-mail additional. Make checks payable to the American Institute of Physics.